Landsc Ecol (2023) 38:1373–1393
https://doi.org/10.1007/s10980-023-01640-y

RESEARCH ARTICLE

A new fractal index to classify forest fragmentation and disorder

Daniel Peptenatu · Ion Andronache · Helmut Ahammer · Marko Radulovic · Jennifer K. Costanza · Herbert F. Jelinek · Antonio Di Ieva · Kohei Koyama · Alexandra Grecu · Andreea Karina Gruia · Adrian-Gabriel Simion · Iulia Daniela Nedelcu · Cosmin Olteanu · Cristian-Constantin Drăghici · Marian Marin · Daniel Constantin Diaconu · Rasmus Fensholt · Erica A. Newman

Received: 6 August 2022 / Accepted: 10 March 2023 / Published online: 7 April 2023

Abstract

Context Forest loss and fragmentation pose extreme threats to biodiversity. Their efficient characterization from remotely sensed data therefore has strong practical implications. Data are often separately analyzed for spatial fragmentation and disorder, but no existing metric simultaneously quantifies both the shape and arrangement of fragments.

Objectives We present a fractal fragmentation and disorder index (FFDI), which advances a previously developed fractal index by merging it with the Rényi information dimension. The FFDI is designed to work across spatial scales, and to efficiently report both the fragmentation of images and their spatial disorder.

Methods We validate the FFDI with 12,600 synthetic hierarchically structured random map (HRM) multiscale images, as well as several other categories of fractal and non-fractal test images (4880 images). We then apply the FFDI to satellite imagery of forest cover for 10 distinct regions of the Romanian Carpathian Mountains from 2000–2021.

Daniel Peptenatu and Ion Andronache have contributed equally to this work.

Supplementary Information The online version contains supplementary material available at https://doi.org/10.1007/s10980-023-01640-y.

D. Peptenatu · I. Andronache · A. Grecu · A. K. Gruia · A.-G. Simion · I. D. Nedelcu · C.-C. Drăghici · M. Marin · D. C. Diaconu
Research Center for Integrated Analysis and Territorial Management, University of Bucharest, Bucharest, Romania
e-mail: daniel.peptenatu@geo.unibuc.ro

I. Andronache
e-mail: ion.andronache@geo.unibuc.ro

A. Grecu
e-mail: alexandra.grecu@faa.unibuc.ro

A. K. Gruia
e-mail: karina.gruia@faa.unibuc.ro

A.-G. Simion
e-mail: simion.adrian14@gmail.com

I. D. Nedelcu
e-mail: iulia.nedelcu9@gmail.com

C.-C. Drăghici
e-mail: cristian.draghici@geo.unibuc.ro

M. Marin
e-mail: marian.marin@geo.unibuc.ro

D. C. Diaconu
e-mail: daniel.diaconu@unibuc.ro

H. Ahammer
GSRC, Division of Medical Physics and Biophysics, Medical University of Graz, Graz, Austria
e-mail: helmut.ahammer@medunigraz.at

M. Radulovic
Department for Experimental Oncology, Institute for Oncology and Radiology of Serbia, Pasterova 14, 11000 Belgrade, Republic of Serbia
e-mail: marko@radulovic.net

Results The FFDI outperformed its two individual components (fractal fragmentation index and Rényi information dimension) in resolving spatial patterns of disorder and fragmentation when tested on HRM classes and other image types. The FFDI thus offers a clear advantage when compared to the individual use of fractal fragmentation index and the Information Dimension, and provided good classification performance in an application to real data.
Conclusions This work improves on previous characterizations of landscape patterns. With the FFDI, scientists will be able to better monitor and understand forest fragmentation from satellite imagery. The FFDI may also find wider applicability in biology wherever image analysis is used.

Keywords Forest fragmentation · Hierarchically structured random maps · Remote sensing · Rényi information dimension · Romanian Carpathian Mountains · Spatial disorder

Introduction

Forested landscapes have complex spatial patterns, and quantification of those patterns has long been of interest for scientists in diverse fields in ecology and beyond (Turner et al. 1989; Wu and David 2002; Newman et al. 2019). Forest loss poses an extreme threat to biodiversity (Haddad et al. 2015; Wilson et al. 2016; Liu et al. 2019). The resulting forest fragmentation produces changes in spatial patterns leading to isolation of patches, habitat degradation, and other ecological processes that further biodiversity loss (Fahrig 2003). Forests support human society through a wide array of functions and processes, each of which may be affected negatively by deforestation, habitat loss, and ecological disruption following fragmentation of habitat. This includes the maintenance of biodiversity (Thompson et al. 2009), stabilizing soils and topography (Mandal and Mondal 2019; Song et al. 2019), regulating stream flows (Cecílio et al. 2019), land surface temperatures (Arroyo-Rodríguez et al. 2017), and acting as carbon sinks mitigating climate change (Bonan 2008; Thompson et al. 2009). Because of forests' many functions, regional patterns and spatial dynamics of forest disturbance and land-use change have global conservation relevance.

Forest fragmentation and land-use change are often assessed by remote sensing (Wickham and Riitters 2019; Fischer et al. 2021; Batar et al. 2021). Although satellite images can be used to easily track the fraction of land usage conversion over time, there is a growing need to quantify temporal and spatial patterns of forest loss. These quantifications are necessary to assess habitat loss and degradation, as well as to predict outcomes such as loss of habitat complexity, biodiversity, or carbon stocks. The fraction of forest cover is one of the variables that can link spatial

J. K. Costanza
USDA Forest Service, Southern Research Station, Research Triangle Park, North Carolina, USA
e-mail: jennifer.costanza@usda.gov

H. F. Jelinek
Department of Biomedical Engineering, Khalifa University, Abu Dhabi, UAE
e-mail: herbert.jelinek@ku.ac.ae

A. Di Ieva
Computational NeuroSurgery (CNS) Lab, Faculty of Medicine, Health and Human Sciences, Macquarie Medical School, Macquarie University, Sydney, NSW, Australia
e-mail: antonio.diieva@mq.edu.au

K. Koyama
Department of Agro-environmental Science, Obihiro University of Agriculture and Veterinary Medicine, Inadacho, Obihiro, Hokkaido 080-8555, Japan
e-mail: koyama.kohei@a.hokkyodai.ac.jp

A. Grecu · A. K. Gruia · C. Olteanu
Faculty of Administration and Business, University of Bucharest, 4-12, 030018 Bucharest, Romania
e-mail: olteanu.cosmin@faa.unibuc.ro

R. Fensholt
Department of Geosciences and Natural Resource Management (IGN), University of Copenhagen, Øster Voldgade 10, 1350 Copenhagen K, Denmark
e-mail: rf@ign.ku.dk

E. A. Newman (✉)
Department of Integrative Biology, University of Texas at Austin, Austin, Texas, USA
e-mail: newmane@berkeley.edu

patterns of land use to their ecological importance, whereas fractal fragmentation analysis and Information Dimension are mathematical tools that have demonstrated utility in analysis of satellite images at multiple spatial scales.

Fractal analysis of fragmentation and information dimension measures of disorder

Fractal analysis is a set of methods that quantifies the complexity of mathematical or physical objects. Connecting ecosystem and biodiversity complexity measures continues to be challenging (Jin et al. 1995; Loke and Chisholm 2022), as is selecting the scale of analysis, when different scales of forest fragmentation are relevant to different organisms and their interactions (Kareiva 1987; Wiens et al. 1993; Boyce et al. 2017). Fractal metrics have the advantages of ease of calculation, as well as scale-invariance (Ma et al. 2009).

Some of the earliest studies that quantified landscape pattern have used forms of fractal analysis, including fractal neutral landscape models (Krummel et al. 1987; Gardner et al. 1987; Milne 1988; Gardner and O'Neill 1991; With and King 1997, 1999), the midpoint displacement method (Barnsley et al. 1988), lacunarity (a fractal method that relies on box counting at different scales) (Plotnick et al. 1993, 1996) and hierarchically structured random maps (Plotnick et al. 1993). Fractal dimension (Mandelbrot 1982; Gao et al. 2019) of the neutral landscape is the foundation of a great variety of models. These include models for source-sink relationships (Milne 1992; With 1997), invasive spread of exotic species (Lavorel and Chesson 1995; With 2002, 2004), edge effects (With and King 1997), and landscape fragmentation and its effects on population and community dynamics (With 2002; With and King 2004). Fractal dimension has also been useful in identifying critical thresholds for correlation of ecological processes with landscape models (Homan et al. 2004; Groffman et al. 2006), characterizing disorder of landscapes (Wimberly 2006) and analysis of dispersion patterns (Walters 2007), including spatial patterns of disturbance (Coops et al. 2018). As useful as fractal analysis has proven, ecological patterns are not truly fractal in the mathematical definition, but are strictly multiscale (Halley et al. 2004). Furthermore, fractal equations tend to be relatively simple and contain very little information about the complex systems they model (Halley et al. 2004; Newman et al. 2019). While fractals were among the earliest algorithms applied in landscape ecology, indices and algorithms developed in recent years that have broader applicability to real ecosystems have largely replaced them (Gustafson 2019; Gao et al. 2019; Turner and Gardner 2015).

Information entropy is a non-fractal approach to quantify the amount of spatial structure or disorder in a matrix of objects. Information entropy has also been used widely in landscape ecology (Nowosad and Stepinski 2019), for example in the study of landslides (Yufeng and Fengxiang 2009; Park 2015), in generating models of species distribution (Phillips et al. 2004; Elith and Leathwick 2009), as an indicator of fragmented landscapes (Joshi et al. 2006), for identification of types of mature woody forest ecosystems (Weber 2011), deriving macroecological patterns (Shipley et al. 2006; Harte and Newman 2014), and for quantification of the effects of disturbance on biodiversity (Supp and Ernest 2014; Newman et al. 2020). The most used form is Shannon information entropy, which measures the average information content in cases when the value of the random variable is not known (Shannon 1948). In this study, we use a generalization of Shannon information called the Rényi information dimension (or "Information Dimension") (Rényi 1970). The Information Dimension is a general way to quantify the diversity, uncertainty, or randomness of a system. The Information Dimension, denoted D_1, measures the fractal dimension of a probability distribution, and relates the rate of growth of Shannon information to how finely the system under study is discretized. This method links scale-dependence and fractal structure to information entropy metrics.

Previous work and the introduction of the FFDI

In this study, we build on the previously developed fractal fragmentation index (FFI) (Andronache et al. 2016), by introducing the fractal fragmentation and disorder index (FFDI). The FFI is an efficient, fractal-based index that determines the degree of fragmentation or compaction of objects based on their shape (Andronache et al. 2016), which is not a feature of classical fractal analysis. The FFI is simply calculated as the dimension of the area minus the dimension of the perimeter of a shape, representing a measure of

occupancy of space ("area" of a fractal can also be called "mass" or "core"). We improved the FFI performance by incorporating the Information Dimension, which further quantifies the spatial distribution of these objects. We observed that FFI does not differentiate patterns where the component objects are extremely small such that no borders can be extracted, or where objects completely fill the space (in which case, FFI = 0, because $D_{area} = D_{perimeter}$). The FFDI was also designed to overcome these limitations by additionally quantifying informational entropy in the image using the Information Dimension (D_1; see Table 1).

The FFI has previously been applied in the analysis of deforestation effects at the county level, territorial administrative units, and mountain groups of Romania (Drăghici et al. 2017; Pintilii et al. 2017; Andronache et al. 2017, 2019; Diaconu et al. 2019), indicating in all cases that fractal fragmentation increases as a result of deforestation. However, deforestation and total habitat loss is not the same as habitat fragmentation per se, so the degree of fragmentation of a landscape only measures one aspect of remaining habitat on landscapes after deforestation (Fahrig 2017). The spatial clustering and organization of the remaining fragments, captured by the Information Dimension, correlates with the distance among patches, which in turn captures ecological processes such as dispersal among patches, or patch isolation (Plotnick et al. 1993). The FFI was also previously tested on synthetically generated hierarchically structured random map (HRM) images, which are characterized by increasing fragmentation and disorder but decreasing average size over multiple scales.

In this paper, we address the limitations of the FFI by developing the fractal fragmentation and disorder index (FFDI), which quantifies the organization and arrangement of objects, thereby providing an estimate of spatial complexity. It can be used for the relative categorization of images with the same size, that is, extent and resolution. We validated the FFDI using several sets of binarized fractal and non-fractal test images, as well as synthetically generated hierarchically structured random maps (HRMs), which are binary maps with known properties, including a specified amount of cover and a hierarchical, nested property of patches (Lavorel et al. 1993; Plotnick et al. 1993). We show the added value of FFDI by demonstrating the complementarity in information content between the measures of fragmentation and disorder (definitions of abbreviations are provided in Table 1). We applied the index to images of forest cover from the Carpathian Mountains of Romania, from the Global Land Analysis and Discovery database (Hansen et al. 2013) (https://glad.earthengine.app/view/global-forest-change; accessed 2020–2022). Finally, we discuss the utility of FFDI for

Table 1 Definitions of terms and abbreviations

Term or abbreviation	Meaning	Definition
Curdling and random trema	From "curdling," meaning nucleation of mass, and "trema" (/ˈtɹɛm.ə/, /ˈtɹiː.mə/), deriving from the Greek word τρῆμα, meaning holes or perforations; in this case, holes of a specified shape in a mathematical surface	A fractal geometry method for generating a mathematical surface with partial surface occupancy
D_1	Rényi information dimension; Information Dimension	D_1 is a fractal dimension that quantifies the amount of spatial structure or disorder in a matrix of objects; it measures the growth rate of Shannon entropy over increasingly finer discretization of space
FFI	Fractal fragmentation index	FFI is a fractal index that quantifies the degree of fragmentation or compaction of an object
FFDI	Fractal fragmentation and disorder index	FFDI is a new index that quantifies the fragmentation/compaction and order/disorder of an object
HRM	Hierarchically structured random map	HRM is a type of image generated by a recursive algorithm derived from a curdling and random trema process

quantification of forest patterns, and more objectively informing forest conservation and policy efforts.

Methods

Defining the fractal fragmentation and disorder index (FFDI)

Because spatial disorder and fragmentation of landscape patterns are often correlated but not perfectly so, a mixed index can quantify these two characteristics in a single value. Spatial disorder refers to the way in which the objects analyzed are organized in space: whether they are arranged with a high level of pattern and order, or alternatively show disorder. Fragmentation, on the other hand, refers to how much the objects analyzed break up a space. If all the space is occupied entirely by a single object, then the image has no fragmentation at all. However, the objects that break up, or "perforate" the image, indicate fragmentation. Fragmentation tends to correlate with coverage (Fig. 1), such that, for example, images with 10% cover are more fragmented, and images with 90% cover are more compact. In the case of a single object, if it is Euclidean, then it is compact, and the more irregular it is, the more fragmented it will be.

The fractal fragmentation and disorder index, or FFDI, is derived from both the fractal fragmentation index (FFI) and the information dimension (D_1) (Fig. 2). Like the FFI, it differentiates spatial organization patterns for processed images that represent two categories (target and non-target). Initial work and limitations of the FFI led us to the testing of a model which includes both FFI and D_1 to explain more than one kind of empirical pattern. We hypothesized that a functional form of FFI multiplied by D_1 would be better able to differentiate compaction/fragmentation and disorder patterns than either metric on its own. In ecology, these patterns of compaction, fragmentation, and disorder could correspond to, for example, natural patchiness of forest habitat, natural patterns of vegetation in response to aridity, or deforested landscapes due to road building and resource extraction. A more informative metric that contains measures of fragmentation and disorder may be better able to quantify these different ecological processes, and be applied in areas where on-the-ground information is not readily obtained.

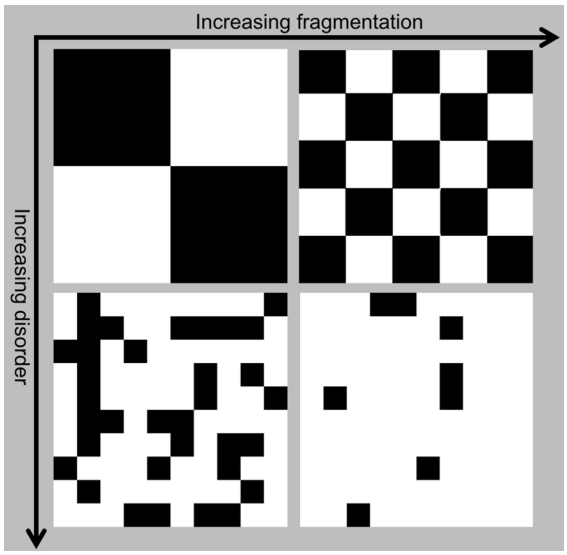

Fig. 1 Schematic of the correlation between disorder and fragmentation. Increasing fragmentation is shown from left to right, and increasing disorder is shown from top to bottom. Black indicates objects, and white indicates background

The Information Dimension is a measure of the amount of "disorder" presented in the image (Bianciardi et al. 2014; de Souza Lins Borba et al. 2016; Borowska et al. 2017). Here, D_1 is derived from the multiscale Rényi entropies. The calculation of the Information Dimension (D_1) is efficiently estimated with a box counting method (Loke and Chisholm 2022), and is initialized with the information entropy (Fig. 2).

The information entropy $I(\varepsilon)$ for a set of $N(\varepsilon)$ boxes of linear size ε is defined as:

$$I(\varepsilon) = -\sum_{i=1}^{N(\varepsilon)} m_i(\varepsilon)\log\left(m_i(\varepsilon)\right). \quad (1)$$

The variable m_i is defined as

$$m_i = \frac{M_i}{M}, \quad (2)$$

where M_i is the number of points in the ith box, and M is the total number of points in the fractal object. Following from these definitions, D_1 is given by the equation (from Baker and Gollub 1996):

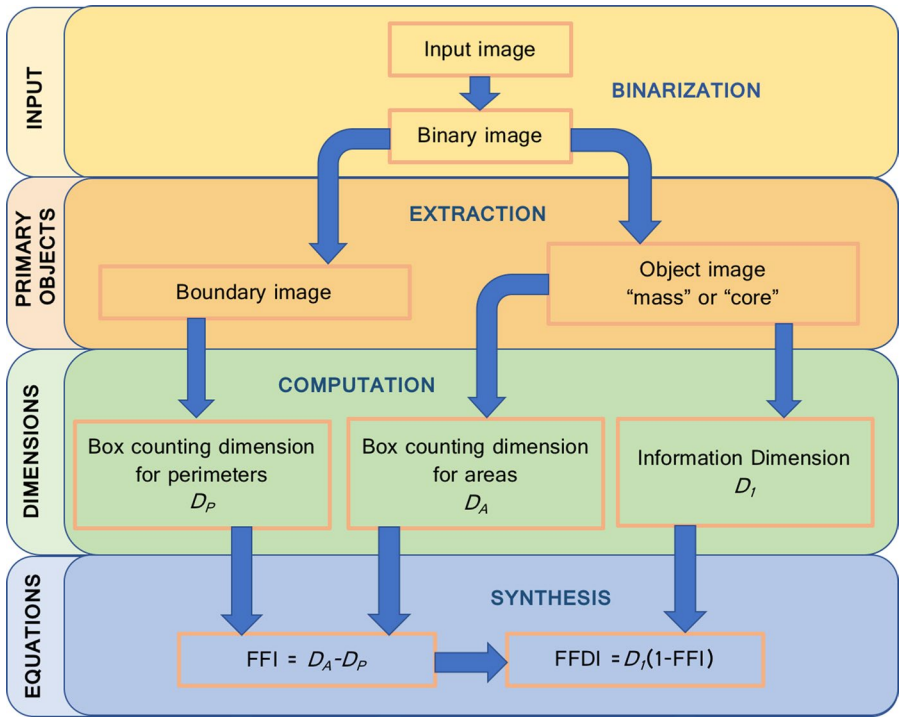

Fig. 2 Workflow diagram for producing both the fractal fragmentation index (FFI) and the fractal fragmentation and disorder index (FFDI)

$$D_1 = \lim_{\varepsilon \to 0} \sum_{i=1}^{N(\varepsilon)} \frac{m_i(\varepsilon)\log\left(m_i(\varepsilon)\right)}{\log(\varepsilon)}. \quad (3)$$

D_1 is measured by overlaying the image with m_i boxes of linear size ε (and area ε^2).

If we consider a set of points distributed evenly in the two-dimensional plane, we will have approximately N number of points:

$$N(\varepsilon) \approx \frac{1}{\varepsilon^2} \text{ and } m_i \approx \varepsilon^2. \quad (4)$$

The area is normalized to unity. Equation (1) therefore becomes:

$$I(\varepsilon) \approx -\frac{1}{\varepsilon^2}\left[2\varepsilon^2 \log(\varepsilon)\right] = -2\log(\varepsilon). \quad (5)$$

For a set of points situated along a smooth line, we get

$$I(\varepsilon) \approx -\log(\varepsilon). \quad (6)$$

And finally, the information dimension can be defined in relation to information entropy as:

$$I(\varepsilon) \approx -D_1 \log(\varepsilon). \quad (7)$$

Information entropy $I(\varepsilon)$ is calculated using Eq. (7). If the set is fractal, then the plot $I(\varepsilon)$ versus $\log(\varepsilon)$ will follow a straight line with a negative slope equal to $-D_1$. The information dimension differs from the box-counting dimension in that it weights the boxes according to the number of points in the boxes, according to Eqs. (1) and (8).

$$N(\varepsilon) = \sum_i m_i(\varepsilon) \quad (8)$$

The information dimension effectively assigns greater weights if a greater number of points are present (Kunicki et al. 2009).

The FFI is an index that describes the degree of fragmentation of objects, but can also be used as a compaction index (Andronache et al. 2016). A smaller FFI indicates more fragmentation and a larger FFI indicates more compaction. The FFI derives from the box-counting fractal analysis for the area of the analyzed objects and perimeter of the same objects, and is calculated:

$$\text{FFI} = D_A - D_P = \lim_{\varepsilon \to 0}\left(\frac{\log N(\varepsilon)}{\log \frac{1}{\varepsilon}}\right) - \lim_{\varepsilon \to 0}\left(\frac{\log N'(\varepsilon)}{\log \frac{1}{\varepsilon}}\right), \quad (9)$$

where FFI is the fractal fragmentation index; D_A is the fractal dimension of the summed areas and D_P is the fractal dimension of the summed perimeters; ε represents the size of the box; $N(\varepsilon)$ represents the number of contiguous and non-overlapping boxes necessary to cover the area of the object; and $N'(\varepsilon)$ represents the number of contiguous and non-overlapping boxes needed to cover only the perimeter of the object (Andronache et al. 2016).

The FFI has the following properties: (1) FFI = 0 is the case when the analyzed objects are very small (in the 1–4-pixel range), such that their contour cannot be extracted, such that $D_A = D_P = 0$; (2) FFI = 1 is calculated when analyzing a 100% compact Euclidean object, without any discontinuity ($D_P = 1$ and $D_A = 2$); (3) when the objects are compact, the FFI value approaches 1, and when they are more fragmented, the FFI value approaches 0. Therefore, the new index FFDI is defined by:

$$\mathrm{FFDI} = D_1(1-\mathrm{FFI}) = \left(\lim_{\varepsilon\to 0}\sum_{i=1}^{N(\varepsilon)}\frac{m_i(\varepsilon)\log\left(m_i(\varepsilon)\right)}{\log(\varepsilon)}\right)\left(1-\left(\lim_{\varepsilon\to 0}\left(\frac{\log N(\varepsilon)}{\log\frac{1}{\varepsilon}}\right)-\lim_{\varepsilon\to 0}\left(\frac{\log N'(\varepsilon)}{\log\frac{1}{\varepsilon}}\right)\right)\right), \tag{10}$$

where $m_{i=}\frac{M_i}{M}$ as defined above, and ε is the size of the box. The slope of the log–log relationship provides the fractal dimension. In this definition, 1-FFI is used because FFI = 0 indicates fragmentation and FFI = 1 indicates lack of fragmentation (Andronache et al. 2016).

While the 1–FFI values range between 0 and 1 and D_1 between 1 and 2, the FFDI range is between 0 and 2, thus allowing a clearer differentiation than the FFI. The maximum value of FFDI approaches 2 when objects are strongly disordered and fragmented, whereas the lowest value approaches 0 when objects are weakly disordered and compact.

To calculate D_1 for the mass of objects, we used built-in tools for the extraction of the primary objects, i.e., the boundary image and mass of the object in the image (Fig. 1). We then employed a built-in algorithm for measuring the global Information Dimension from the Rényi family of fractal dimensions

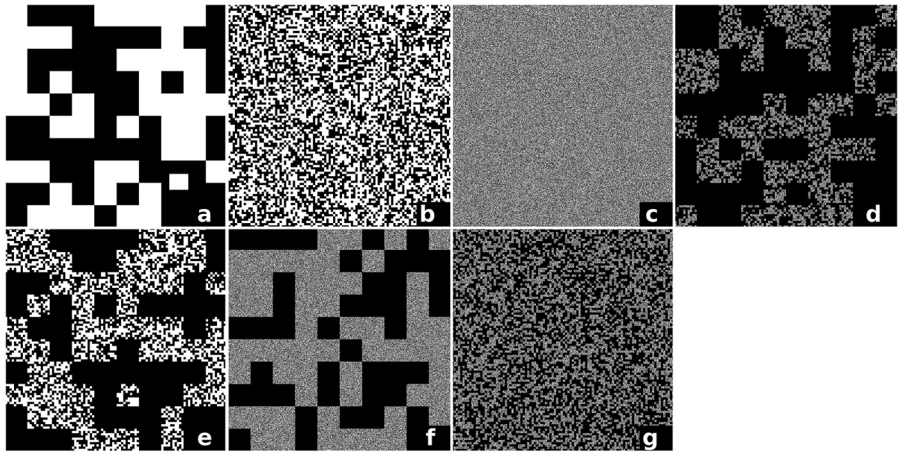

Fig. 3 Examples of hierarchically structured random map (HRM) images generated: **a** high s_1 set ($p_1 = 0.5$ and $p_3 = p_2 = 1$), **b** middle s_2 set ($p_2 = 0.5$ and $p_1 = p_3 = 1$), **c** low s_3 set ($p_3 = 0.5$ and $p_1 = p_2 = 1$), and several combined sets: **d** mixed s_4 set ($p_1 = p_2 = p_3 = 0.5$), **e** high + middle $s_1 + s_2$ set ($p_1 = p_2 = 0.5$ and $p_3 = 1$), **f** high + low $s_1 + s_3$ set ($p_1 = p_3 = 0.5$ and $p_2 = 1$) and **g** middle + low $s_1 + s_3$ set ($p_2 = p_3 = 0.5$ and $p_1 = 1$). For the s_1 images with $p_2 = p_3 = 1$ and $p_1 = 0.5$, 50% of the space is randomly occupied by HRM objects sized 100 × 100 pixels. For the s_2 images with $p_1 = p_3 = 1$ and $p_2 = 0.5$, 50% of the space is randomly occupied by HRM objects sized 10 × 10 pixels. For the s_3 images with $p_1 = p_2 = 1$ and $p_3 = 0.5$, 50% of the space is randomly occupied by HRM objects sized 1 × 1 pixel. In the case of s_4 images, $p_1 = p_2 = p_3 = 0.5$, which represent images where 50% of the space contains HRM objects sized 100 × 100 pixels (s_1), 10 × 10 pixels (s_2), and 1 × 1 pixel (s_3)

available in the open-source plugin ComsystanJ 2.0.1 (Ahammer 2011) for the Java-based open-source software Fiji. The ComsystanJ box-counting dimension method was used to calculate both the FFDI and FFI.

Generation of hierarchically structured random map images for testing FFDI

HRMs are maps of pixels that are randomly set to 1 or 0, with probability distributions of 1's and 0's that vary by region. HRMs can simulate landscapes that have different levels of clustering and fragmentation, which is accomplished by curdling and random trema. Two surfaces can have the same total amount of filled space, but differ in their level of curdling, that is, the clustering or nucleation of the filled space. The non-filled space is generated by random trema, or randomly placed holes of a given shape in the mathematical surface (Mandelbrot 1982; Gardner et al. 1987; Milne 1992). For this study, HRM images were generated by the Fiji plugin ComsystanJ using a recursive algorithm derived from the curdling and random trema generation method employed by Plotnick (Mandelbrot 1982; Plotnick et al. 1993). Note that for studies that compare images, all images should have the same resolution (pixel size) and extent, in order to avoid introducing bias from automatic resizing and other sources of error (Loke and Chisholm 2022). This applies both to images generated algorithmically and to images processed from empirical data.

The HRM images were generated for our tests with numbers of rows and columns (M) fixed at 1000 (1,000,000 pixels; or 1000 × 1000-pixel resolution). Variables p_1, p_2 and p_3 represent the percentage of space occupied by the HRM objects at different grain sizes (e.g. 0.5 = 50%). These were generated by creating arrays with L rows and L columns and randomly setting the L^2 elements to 1 with a probability p', with p_1, p_2 and p_3, representing the percentage of space occupied by the HRM objects at different scales. For p_1, the size of the generated HRM objects is at 100 × 100 pixels grain; for p_2 it is 10 × 10 pixels; and for p_3 it is 1 × 1 pixel. In each case, p', the total filled area of the image, is 0.5 (i.e. 50%) for each type of HRM object generated. Due to their random distribution, the images are evenly occupied by HRM objects (Fig. 3).

We generated seven sets of 2D HRMs synthetic images with different values of p_1, p_2 and p_3, labeled s_1, s_2, s_3, s_4, $s_5 = s_{1+2}$, $s_6 = s_{1+3}$ and $s_7 = s_{2+3}$. Following the p_1–p_3 designations, the s_1–s_3 sets are each characterized by a single "grain size": s_1 being the "high" set of 100 × 100 pixels grain size, s_2 being the "medium" set of 10 × 10 pixels, and s_3 being the "low" set of 1 × 1 pixel grain size. The remaining s_4–s_7 sets were "mixed" sets with combinations of the high, medium, and low sets. We then calculated the FFI, D_I, and FFDI for these images to compare the performance of the different metrics.

For each of the seven sets of images, we generated 200 images at each level of coverage that was varied for that set. This resulted in 12,600 HRMs (Supplementary Information 1), including nine classes for the "high" set of images (s_1) with $p_1 = 0.1, 0.2, \ldots, 0.9$ and $p_2 = p_3 = 1$; nine classes for the "middle" set (s_2) with $p_1 = p_3 = 1$ and $p_2 = 0.1, 0.2, \ldots, 0.9$; nine classes for the "low" set (s_3) with $p_1 = p_2 = 1$ and $p_3 = 0.1, 0.2, \ldots, 0.9$; and nine classes for a "mixed" set (s_4) with $p_1 = p_2 = p_3 = 0.1, 0.2, \ldots, 0.9$. Similarly, we generated nine classes for the "high-middle" set ($s_1 + s_2$) with $p_1 = p_2 = 0.1, 0.2, \ldots, 0.9$ and $p_3 = 1$, nine classes for the "high-low" set ($s_{1+}s_3$) with $p_2 = 1$ and $p_1 = p_3 = 0.1, 0.2, \ldots, 0.9$, and nine classes for the "middle-low" set (s_3) with $p_1 = 1$ and $p_2 = p_3 = 0.1, 0.2, \ldots, 0.9$ (Fig. 3).

Although the exact levels of fragmentation and disorder vary, even among images with the same levels of p_1, p_2 and p_3, we can say general things about the image classes before analyzing them, based on the definitions of fragmentation and disorder. Images in the s_1 class are characterized by large, compact HRM objects with less disordered spatial distribution; s_2 and $s_1 + s_2$ images by medium-sized HRM objects with moderate fragmentation and spatial disorder; while images in the s_3 set are very fragmented and their distribution highly disordered. The s_4 set images include s_1, s_2, and s_3 HRM objects and are obtained by filling the space with HRM objects from the s_1 and s_2 image sets and fractal spaces from the s_2 with s_3 HRM objects. Therefore, s_4 is fragmented

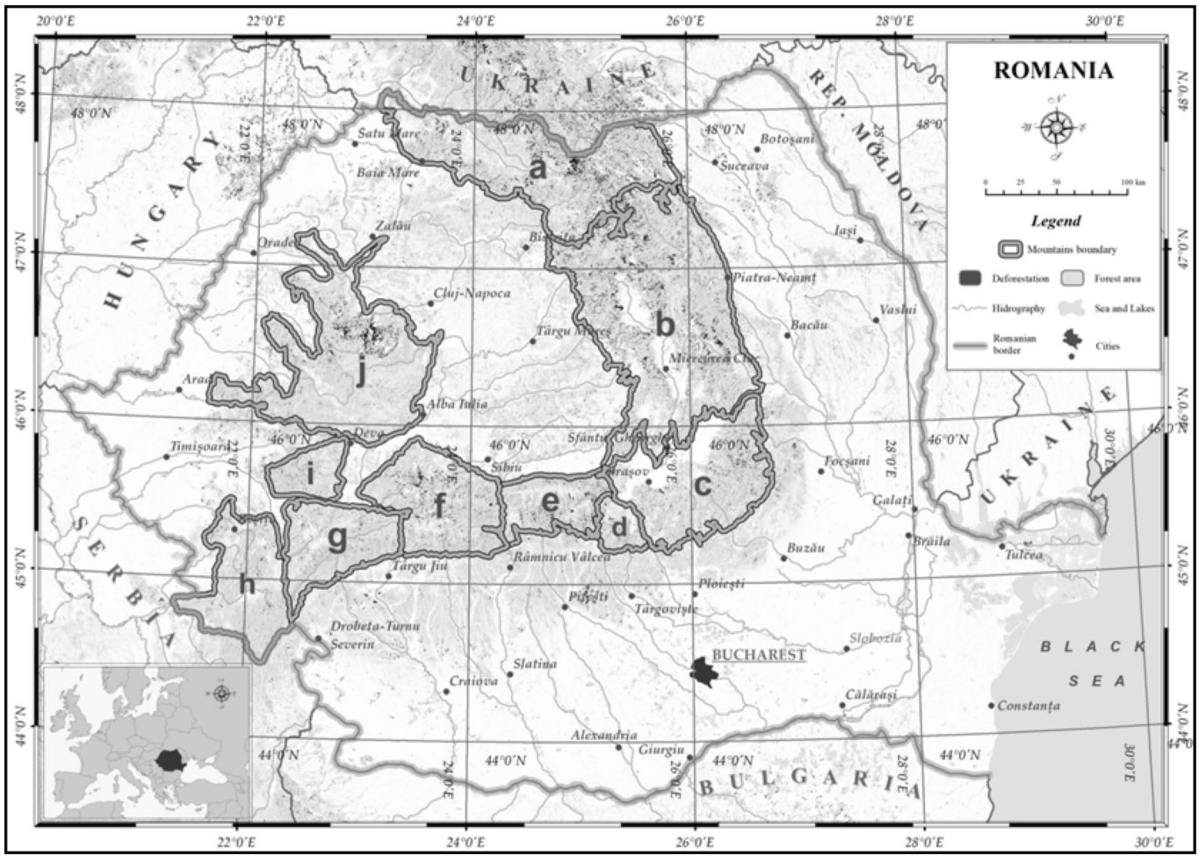

Fig. 4 The geographic location of the study area, indicating **a** Northern group of Oriental Carpathians; **b** Central group of Oriental Carpathians; **c** Southern group of Oriental Carpathians; **d** Bucegi Mountains Group; **e** Făgăraș Mountains Group; **f** Parâng Mountains Group; **g** Retezat–Godeanu Mountains Group; **h** Banat Mountains; **i** Poiana Ruscă Mountains and **j** Apuseni Mountains. Compass points are approximate over the regional extent given the map projection

and disordered. The most fragmented and disordered images are the $s_1 + s_3$ and $s_2 + s_3$ sets of images.

Generation of fractal and non-fractal validation images

Using the ComsystanJ plugin, we also generated 24×200-image sets of gray-scale images for validating the FFDI (4800 images in total). We generated eleven sets of images with midpoint displacement (MDP) with fractal dimension FD = 2.0, FD = 2.1, ..., FD = 3.0. We also generated eleven sets of fast Fourier transform (FFT) images: FD = 2.0, 2.1, ..., 3.0; random images; and Gaussian algorithms. All images were binarized using ImageJ 1.5.2 software (Schneider et al. 2012; Kainz et al. 2015).

For FFDI validation, we generated 20 horizontal sinusoidal images with an increasing number of iterations, from 1–20; 20 vertical sinusoidal images generated with 1–20 iterations; 20 radial sinusoidal images generated with 1–20 iterations; 10 IFS Sierpiński Gasket images generated with 0–9 iterations; and 10 IFS Menger Carpet images generated with 0–9 iterations (80 images total). All testing and validation images generated for this study are provided in the Supplementary Information 1–4.

Case study: dynamics of forest loss in the Romanian Carpathians

To test the proposed FFDI in a real-world setting, we analyzed the dynamics of forest loss and the impact

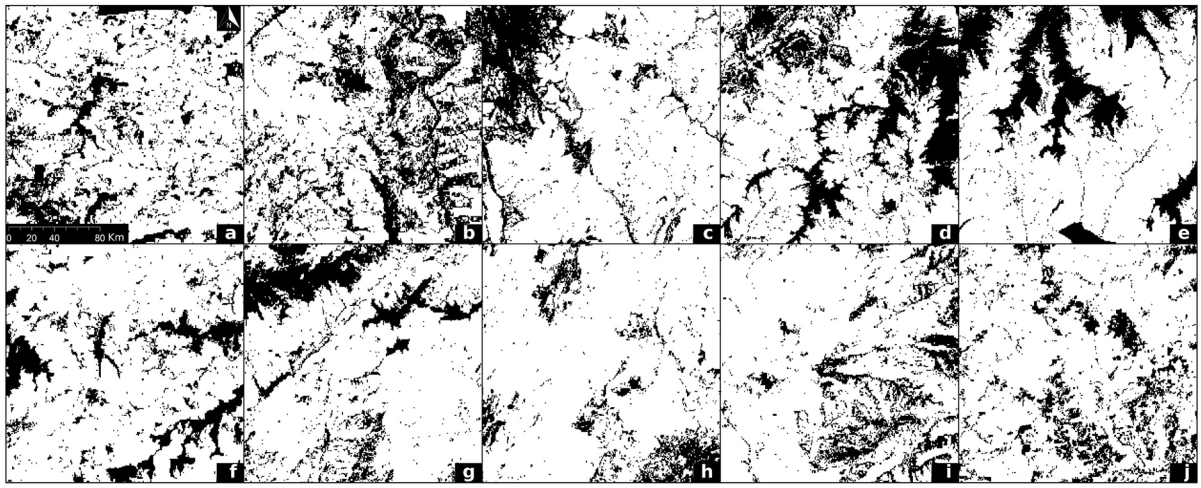

Fig. 5 Examples of tree cover binary images (from 2000 CE): **a** Northern group of Oriental Carpathians; **b** Central group of Oriental Carpathians; **c** Southern group of Oriental Carpathians; **d** Bucegi Mountains Group; **e** Făgăraș Mountains Group; **f** Parâng Mountains Group; **g** Retezat–Godeanu Mountains Group; **h** Banat Mountains; **i** Poiana Ruscă Mountains and **j** Apuseni Mountains. The dimensions of all images are 1000 × 1000 pixels. White pixels correspond to forest cover and black pixels correspond to non-forest cover

of forest dynamics in the Romanian Carpathian Mountains. The study area constitutes a major landscape unit with mountainous features, which forms a circular arc from the border with Ukraine in the north of the country to the border with Serbia in the south (Fig. 4).

Geological and geomorphological features divide the Carpathians into three major sectors (the Eastern Carpathians, the Southern Carpathians and the Western Carpathians). Each sector is divided into 10 more-or-less coherent mountain groups, depending on the degree of forest fragmentation, controlled by the geology and the cross-sectional valley corridors (Fig. 4). The Eastern Carpathians include the Northern, Central and Curvatures Groups. The Bucegi, Făgăraș, Parâng and Retezat-Godeanu Mountains belong to the Southern Carpathians, whereas the Apuseni, Poiana Ruscă and Banat Mountains are a part of the Western Carpathians. Their average elevation is ~ 2000 m, and the absolute maximum elevation is the Moldoveanu Peak in the Făgăraș Mountains (2544 m) (Balteanu et al. 1998).

In comparison to the situation at the global level (Song et al. 2018), the deforestation in Romania shows continuous growth (Andronache et al. 2019). The 2017 Report on the State of the Forests of Romania states that in that year, forests of Romania occupied an area of 6,565,000 ha, or 27.5% of the country's land area. Although deforestation has increased in total during recent decades, areas of forest loss have been partly compensated for by forest regeneration, reforestation, refurbishment of forested pastures and the inclusion of degraded lands in afforestation efforts, aligned with the provisions of Law no. 46/2008 (Ministry of Water and Forests 2017).

Forest image preprocessing

The Global Forest Change database used in the current research is based on Landsat satellite time series data, provided by the Geographical Sciences Department at the University of Maryland, College Park. The data set provided is based on a change detection analysis, which highlights year-to-year forest dynamics since the year 2000 CE. We therefore chose the year 2000 to be used as the base year for which the rest of the analysis is reported.

Forest cover images for Romania were downloaded with 30 m spatial resolution in GeoTIFF format from the Global Forest Change database. Total tree cover for the year 2000 was used as a baseline comparison for forest loss for each year from 2001 to 2021. Subsets of forest loss area images for each of the 21 years were generated for each of the mountain groups, for subsequent binarization and analysis.

We calculated differences among the images of tree cover for the year of interest and the base year, 2000, to determine area of forest loss for individual years and the cumulative forest loss (using the ImageJ 1.52 Process and Image Calculator functions). Subsequent processing of satellite imagery for extraction of annual images and preparation for the fractal analysis was performed with ArcGIS software (ESRI 2020) (Fig. 5). The grayscale GeoTIFF images were converted to 8-bit TIFF binary images, compatible with binary fractal analysis. Binarization was done using the Threshold operator in the Image-Adjust menu in ImageJ, with the thresholds being 1 and 255. Two classes of pixels resulted: black pixels, with value 0 representing the background and white pixels with value 255, representing the foreground and the objects to be analyzed respectively. In our case, these correspond to patches of forest and deforested areas.

Statistics for images and metrics

In order to apply the FFDI, we first took into account the sample size and the general rule that box counting using at least ten box sizes should be obtained over the scaling range (Kenkel 2013), where the number of boxes was the number of distinct scales of pixels differing by a power of 2 (because "fractal analysis" for empirical images is technically multiscale analysis). Thus, for our fractal analysis, the image resolution

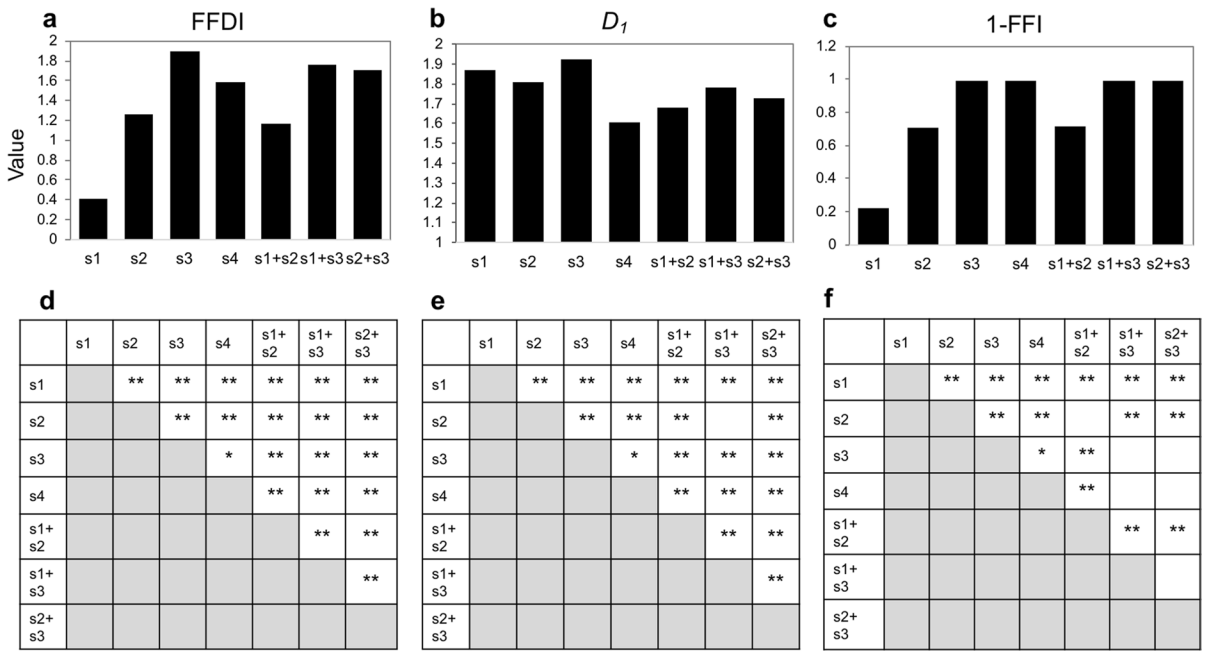

Fig. 6 Statistical analysis of discrimination among HRM images for seven test image sets s_1–s_7, across three metrics: **a** the Fractal Fragmentation and Disorder Index (FFDI); **b** Rényi information dimension (D_1) (note: x-axis does not cross at 0); and **c** 1-the Fractal Fragmentation Index (1-FFI). Values on y-axis are dimensionless. The sample size for each of the HRM image sets is n=1800. Also shown: the $p<0.01$ Kruskal–Wallis test significance matrices for: **d** the FFDI, **e** D_1, and **f** 1-FFI. Pairwise post-hoc tests are Bonferroni corrected (*$p<0.05$, **$p<0.001$) in all cases

allowed us to set the number of boxes to 11, with the regression ranging from 1 (min) to 11 (max).

Second, we checked that the images were sufficiently fractal-like that we could calculate the metrics D_A, D_P, and D_1. According to Benguigui et al. (2000), the quality of the fractal dimension estimation is controlled by using the Pearson correlation coefficient r, and estimations can be accepted when r exceeds the value of 0.99. If the fit between the empirical curve and the estimated curve is low, it can be concluded that either the pattern being studied is not fractal, or that it is multi-fractal (Tannier and Pumain 2005). For the images of the Romanian Carpathians as well as all the test images, we performed preliminary analyses (in ComsystanJ) and found that the coefficient of determination, R^2, was greater than 0.99, and in the case of a linear regression, $R^2 = r^2$. This constrains the Pearson correlation coefficient to be greater than 0.99, so we were able to perform the fractal analyses on the images.

We note that high R^2 values do not always and in general correspond to high linearity. We therefore tested the linear regressions for several box size ranges, from 2^0–2^6 up to 2^0–2^{10} (measured in pixels), and compared the gained results to each other. This was done for all images s_1, s_2, s_3, s_4, s_1+s_2, s_1+s_3, s_2+s_3, Gaussian, Random, FFT, and MPD (with FD ranging from 2.0 to 3.0). The correlations between these results were very high (e.g. $R^2 = 0.996$ between 2^0–2^9 and 2^0–2^{11}, and $R^2 = 0.958$ between 2^0–2^6 and 2^0–2^{11}), with only the absolute values deceasing slightly for smaller box size ranges. This decrease was negligible and did not affect the outcome of this study. Differences between HRM, FFT and MPD images were maintained. Final results were obtained with a range of 2^0–2^{11}, although a smaller range would have been acceptable as well.

Statistical analyses were carried out with SPSS 27 (IBM Corp 2017). Data distributions were tested for normality using Shapiro–Wilk tests ($p < 0.05$). Not all distributions were normally distributed. Thus, non-parametric Kruskal–Wallis tests including Bonferroni corrected post hoc tests were applied.

Results

Evaluation of the FFDI using HRM images

We calculated the FFDI, 1-FFI, and D_I for all the HRM image groups to compare the outcomes of each metric, and their ability to differentiate among image classes. Objects that have high fragmentation are usually spatially disordered, and the most compact objects are usually uniformly spatially distributed. Moreover, when fragmentation is very high, FFI cannot identify patterns (Andronache et al. 2016, 2017). As stated previously, a very high level of fragmentation (FFI near 0) is achieved when images have objects of size 1, or they have very few pixels such that no border can be extracted. In the first stage of fractal analysis, the three algorithms used (1-FFI, D_1 and FFDI) were tested in the three-level HRM images (Fig. 3).

The distributions of 1-FFI, D_I and FFDI values were compared for each of the 9×200 generated images in the high, medium, low, mixed, high-medium, high-low and medium–low HRM sets (Fig. 6). In each case, every metric yields a clear differentiation among the distinct HRM image sets with a sample size of $n = 1800$, with FFDI offering the best differentiation when considering all comparisons, as assessed by Bonferroni-corrected Kruskal–Wallis significance tests. The number of statistically different pairs varied for each of the three metrics. From 21 possible pairs, the FFDI yielded 20 highly significant pairs and one significant pair (Fig. 6a, d). D_I yielded 19 highly significant pairs and one significant pair (Fig. 6b, e). 1-FFI yielded 14 highly significant pairs and again one significant pair (Fig. 6c, f).

Along with the highest number of statistically significant test results, the FFDI also had the highest value variabilities, of 4795%, 81.3%, 15.5%, 139.3%, 65.4%, 46.4% and 60.1%, among synthetic images in s_1, s_2, s_3, s_4, s_{1+2}, s_{1+3}, and s_{2+3}, respectively, while 1-FFI achieved 3354%, 116%, 7.7%, 7.1%, 108,6%, 7.6% and 7.1%. Information Dimension D_1 was the poorest discriminator by relative value distances of 23%, 34.3%, 15.5%, 149.7%, 89.8%, 48.2% and 65.4% for image sets.

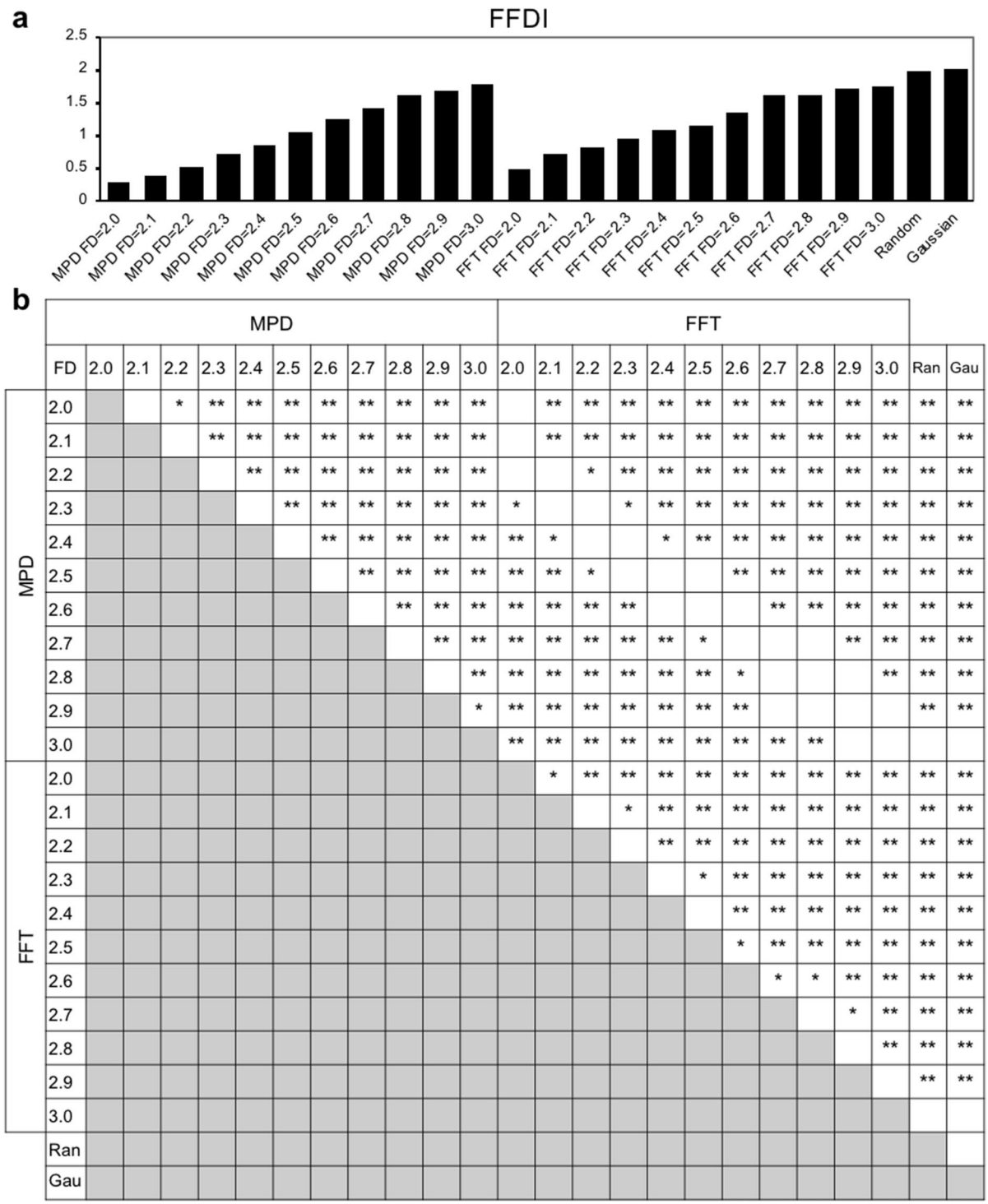

Fig. 7 Statistical analysis of discrimination among binarized test images generated by Midpoint displacement (MPD), fast Fourier transform (FFT), Random, and Gaussian algorithms, with a range of fractal dimensions (FD), for the fractal fragmentation and disorder index (FFDI). **a** For FFDI, values on the y-axis are dimensionless. **b** Comparisons are demonstrated with the $p < 0.01$ Kruskal–Wallis test significance matrix, with Bonferroni corrected pairwise post hoc tests ($*p < 0.05$, $**p < 0.001$)

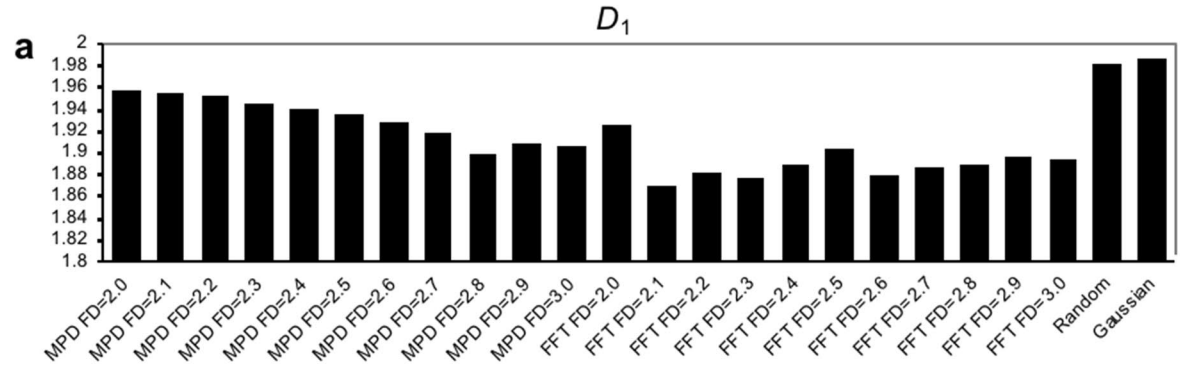

b

		MPD											FFT											
	FD	2.0	2.1	2.2	2.3	2.4	2.5	2.6	2.7	2.8	2.9	3.0	2.0	2.1	2.2	2.3	2.4	2.5	2.6	2.7	2.8	2.9	3.0	Ran	Gau
MPD	2.0					*	*	**	**	**	**	**	**	**	**	**	**	**	**	**	**	**	**	**	**
MPD	2.1						*	**	**	**	**	**	**	**	**	**	**	**	**	**	**	**	**	**	**
MPD	2.2							**	**	**	**	**	**	**	**	**	**	**	**	**	**	**	**	**	**
MPD	2.3							*	**	**	**	**	*	**	**	**	**	**	**	**	**	**	**	**	**
MPD	2.4								**	**	**	**		**	**	**	**	**	**	**	**	**	**	**	**
MPD	2.5								**	**	**	**		**	**	**	**	**	**	**	**	**	**	**	**
MPD	2.6									**	**	**		**	**	**	**	**	**	**	**	**	**	**	**
MPD	2.7													**	**	**	**	*	**	**	**	**	**	**	**
MPD	2.8												**	*		*			**	*	*		*	**	**
MPD	2.9												**	**		**	*		**	*	*		*	**	**
MPD	3.0												**	*		*			**	*	**		*	**	**
FFT	2.0													**	**	**	**	**	**	**	*	**	**	**	**
FFT	2.1																							**	**
FFT	2.2																							**	**
FFT	2.3																							**	**
FFT	2.4																							**	**
FFT	2.5																		*					**	**
FFT	2.6																							**	**
FFT	2.7																							**	**
FFT	2.8																							**	**
FFT	2.9																							**	**
FFT	3.0																							**	**
	Ran																								
	Gau																								

◂**Fig. 8** Statistical analysis of discrimination among binarized test images generated by Midpoint displacement (MPD), fast Fourier transform (FFT), Random, and Gaussian algorithms, with different fractal dimensions (FD), for the Rényi information dimension (D_1) (note: x-axis does not cross at 0). **a** For D_1, values on y-axis are dimensionless. **b** Comparisons are demonstrated with the $p < 0.01$ Kruskal–Wallis test significance matrix, with Bonferroni corrected pairwise post hoc tests (*$p < 0.05$, **$p < 0.001$)

As expected, D_1 differentiated the four classes of image sets with different amounts of disorder, and identified an increasing disorder progressively from s_1 (1.89) to s_3 (1.98). 1-FFI identified the fragmentation differences, indicating that fractal fragmentation decreases when comparing the s_1 set of images (0.24) to the s_3 and s_4 sets of images (0.999). FFDI values increased by 342.9% from the compact and less disordered s_1 set (FFDI = 0.45) to the highly fragmented and more pronouncedly disordered s_3 image set (1.98).

A linear regression with all 12,600 HRM images shows a very low correlation between disorder and fragmentation ($R^2 = 0.075$) in the synthetic images. The FFDI shows a very low correlation with D_1 of $R^2 = 0.017$ and a strong correlation with 1-FFI of $R^2 = 0.837$ in the synthetic images. Due to higher overall discrimination ability, FFDI is expected to work better than the comparison metrics at lower sample sizes.

Evaluation of the FFDI using non-fractal test images

Additional test images were generated by Midpoint displacement (MPD), fast Fourier transform (FFT), Random, and Gaussian algorithms, with different fractal dimensions (FD). As expected, the midpoint displacement and fast Fourier transform algorithms yielded nearly identical images, and thus showed high correlation. On the other hand, the random and Gaussian images had substantially different patterns, without significant correlation. Statistical analyses of discrimination among test images yield very high significances between the distinct fractal dimensions of MPD and FFT generated and binarized images. From 276 possible pairs, the FFDI yields 212 highly significant pairs and 17 significant pairs (Fig. 7). D_1 yields 174 highly significant pairs and 20 significant pairs (Fig. 8). 1-FFI yields 213 highly significant pairs and again 12 significant pairs (Fig. 9). Thus, there are again more significant pairs for FFDI compared to D_1 and 1-FFI.

Several other sets of test images were analyzed as well: horizontal sinusoidal, vertical sinusoidal and radial sinusoidal images with 1–20 iterations; and Menger Carpet and Sierpiński Gasket images with 0–9 iterations. For these images, the value of the FFDI generally increased with the number of iterations, indicating that both the resolution and depth of scale affected the calculated FFDI values (Supplementary Information 5).

Using FFDI to analyze tree cover and forest loss in the Romanian Carpathians

As a practical application, we analyzed and differentiated forest characteristics concerning disorder, and fragmentation of forest cover area (Fig. 10a), total area of loss in the year analyzed (Fig. 10b), and for the cumulative loss area in the Romanian Carpathian Mountains from 2000 to 2021 (Fig. 10c). The FFDI differentiated among three patterns of mountain groups, based on their fragmentation and disorder: the highest values of FFDI (Central, Northern, and Parâng mountain groups) coincided with high fragmentation in the images, which also corresponded to areas of intense deforestation (Fig. 10a). The natural fragmentation and compaction of this landscape lead to the construction of access roads into the forest for resources, which intensifies deforestation pressures. These characteristics and values of fractal measures were very similar to the s_4 set of HRM generated images (Fig. 3). Intermediate values of FFDI (Apuseni, Bucegi, Făgăraș, Poiana Ruscă, and Godeanu mountain groups) were specific for mountain groups with moderate fragmentation and disorder. The lower values of FFDI (Banat, Retezat-Godeanu, and Southern Group mountains) were specific to mountain groups characterized by a higher degree of mountain terrain continuity and lower fragmentation of terrain (relief), implicitly favoring a stronger compaction of forests. This pattern resembled the s_2 "middle" set of HRM images. These patterns agree with previously described patterns of deforestation and fragmentation (Andronache et al. 2019).

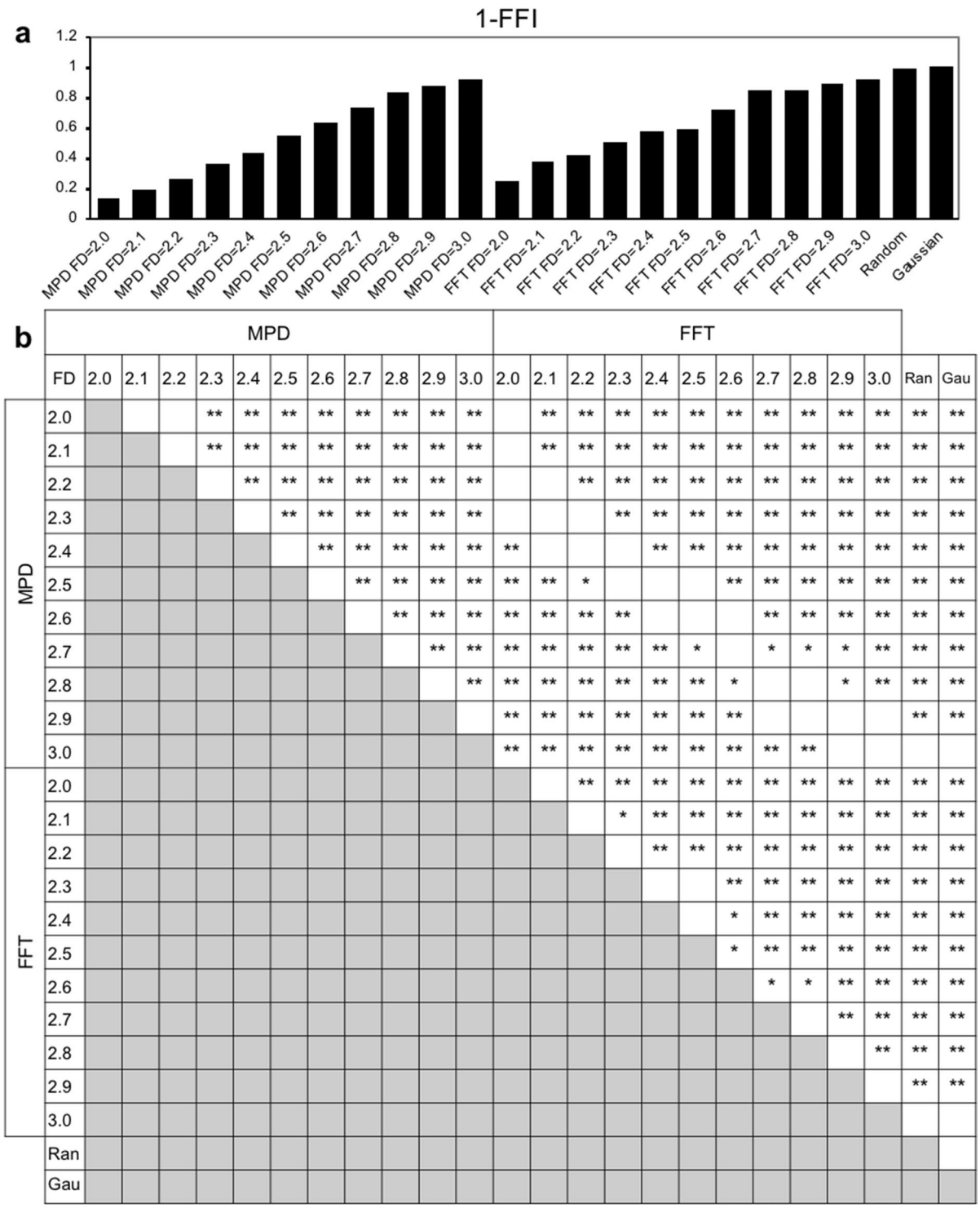

Fig. 9 Statistical analysis of discrimination among binarized test images generated by Midpoint displacement (MPD), fast Fourier transform (FFT), Random, and Gaussian algorithms, with different fractal dimensions (FD), for 1-the fractal fragmentation index (1-FFI). **a** For 1-FFI, values on y-axis are dimensionless. **b** Comparisons are demonstrated with the $p < 0.01$ Kruskal–Wallis test significance matrix, with Bonferroni corrected pairwise post hoc tests (*$p < 0.05$, **$p < 0.001$)

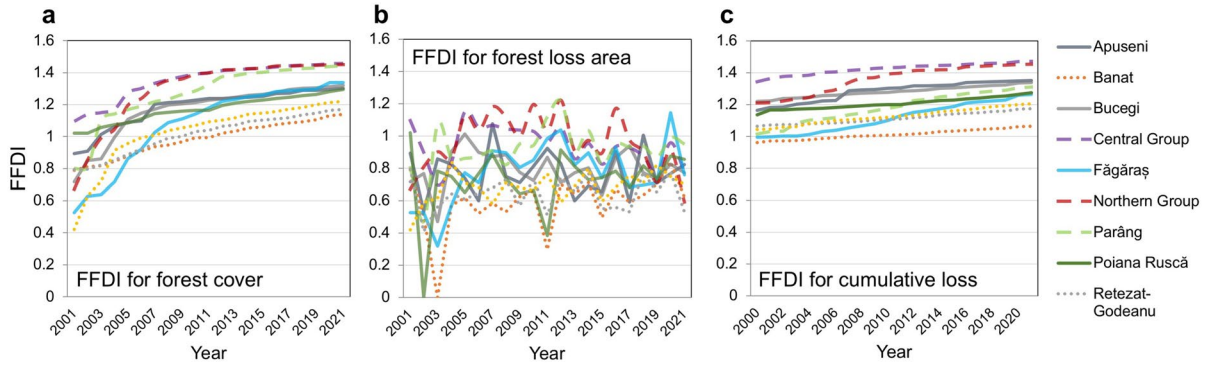

Fig. 10 The compaction and disorder patterns of forest cover and loss in the Romanian Carpathians as represented by the fractal fragmentation and disorder index (FFDI): **a** forest cover areas, **b** forest loss areas, and **c** cumulative loss areas. The highly fragmented and disordered patterns are depicted with dashed lines (Central, Northern, and Parâng mountain groups); the moderately fragmented and disordered patterns are represented with solid lines (Apuseni, Bucegi, Făgăraș, Poiana Ruscă, and Godeanu mountain groups), and the images with lowest fragmentation and disorder are represented with dotted lines (Banat, Retezat-Godeanu, and Southern Group mountains). These patterns agree with some previously described patterns of deforestation and fragmentation (Andronache et al. 2019)

Figure 10c shows a clear increase in FFDI values associated with the areas of cumulative loss over time, which is reflected in the different range of values for the ten mountain groups. In these cases, FFDI increased with increasing loss of forests, because the cumulative loss areas became fragmented and disordered as they expand. We note that for the Făgăraș and Parâng Mountains Groups the cumulative forest loss is increasingly disordered, even though the forest loss areas are not as naturally fragmented as the other three mountain groups from the highly fragmented pattern. Low FFDI values were found for the third pattern of cumulative loss areas due to deforestation patches being very small but numerous, with less disordered spatial distribution (Ciobotaru et al. 2019).

Interestingly, due to very low FFDI values and similar fragmentation of forest loss areas in all 10 mountain groups (Fig. 5), Information Dimension was found to be the measure that could differentiate among these three structural types of mountain groups, similar to the s_4 and s_3 sets of HRM images. With further investigation, the influence of FFI on the FFDI was very small when similar images of mountain groups or structural types are analyzed, similar to s_3 or s_4 HRM images when FFI < 0.006, but becomes important when FFI exceeds 0.1, as is the case for s_1 and s_2 HRM images.

Discussion

Quantifying the spatial structure of landscapes is the key to understanding the ecological effects of landscape patterns and habitat fragmentation (Costanza et al. 2019). Metrics based on fractal analysis are commonly used because of ease of their calculation and multiscale properties. However, another ecologically relevant pattern of the arrangement of habitat fragments, or "landscape disorder," had not been previously measured in fractal-based landscape metrics. Consequently, we formulated a new metric called the Fractal Fragmentation and Disorder Index, or FFDI, that can identify and also classify patterns and subpatterns of image spatial fragmentation and disorder.

In this study, we showed that FFDI outperforms various other metrics in quantifying both fragmentation and disorder of images and solves a previous limitation of the FFI specific to images with highly fragmented, spatially distributed objects. We demonstrated the ability of FFDI to better differentiate and classify HRM patterns compared to fractal fragmentation or Information Dimension, and that this index could be used in the future as a versatile and accurate tool for pattern differentiation and sub-patterns in any field that uses binary imaging. The FFDI performed well in the classification of spatial characteristics of artificially synthesized HRM objects as well as images of real forest patches.

We recognize a limitation in the method applied here that arises as a result of binarization of images to be analyzed with the FFDI. Depending on the chosen threshold, binarization may introduce analytical bias (Eguiraun et al. 2014); however, this effect can be investigated further and might be rectified with the incorporation of a scaling relationship, or use of the FFDI as a relative index for comparison of different system states, rather than as an absolute measure of fragmentation and disorder. Even with this limitation, FFDI offers a clearer differentiation in categorizing synthetic images and in real applications.

Compared to D_1 and FFI, the FFDI achieved a clearer differentiation of forest tree cover, cumulative forest loss and annual forest loss patterns for the 10 mountain groups in the Romanian Carpathians. It is therefore a promising approach for differentiating patterns of deforestation and regrowth and will be useful in environmental monitoring and protection.

In conclusion, although FFDI was developed with the aim to improve the understanding of forest fragmentation, it might be applied generally to landscape fragmentation resulting from urban development, wildfires, and other natural and anthropogenic phenomena. FFDI can also be used for comparative analyses across different regions. We demonstrated the use of the FFDI in estimation fractal dimension as a tool for relative classification of images of the same size and resolution, based on their fragmentation and disorder.

We expect a broad applicability of the FFDI in various disciplines of medicine or biology. For example, in histological slides, the distribution of cells or cell nuclei shows a fragmented pattern which is often irregular or random due to the underlying nonlinear dynamics of gene regulation and cell differentiation (Fabrizii et al. 2014). Improved quantification of such patterns could improve diagnosis, prognosis and prediction in cancer patients. (Macaluso et al. 2015).

Acknowledgements The authors thank Dr. Volker C. Radeloff for his valuable comments and suggestions on an earlier version of this manuscript, and J. Onland for phonemic transcription.

Authors' contributions IA and DP conceptualization; IA, HA, and A-GS methodology; C-CD, KK, MR, HFJ, HA, AKG validation; IA, DP, AG, IDN, AKG formal analysis; C-CD investigation; OD and DCD data curation; IA, DCD, DP, OD, EAN writing—original draft preparation; EAN, JC, RF and MM writing—review and editing; A-GS, EAN visualization; HA, MR, EAN, HFJ, KK and RF supervision. These authors contributed equally to this work: IA, DP.

Funding Research was supported by a grant of the Romanian Ministry of Education and Research, CNCS–UEFISCDI, Project Number PN-III-P4-ID-PCE-2020-1076, within PNCDI III, grant of the Ministry of Research, Innovation and Digitization, CNCS/CCCDI-UEFISCDI, Project Number PN-III-P2-2.1-SOL-2021-0084, within PNCDI III, grant of the University of Bucharest "Spatial projection of the human pressure on forest ecosystems in Romania", University of Bucharest, (UB/1365) and grant "Development of the theory of the dynamic context by analyzing the role of the aridization in generating and amplifying the regressive phenomena from the territorial systems", Executive Agency for Higher Education, Research, Development and Innovation Funding, Romanian Ministry of Education Research Youth and Sport (UEFISCDI) (TE-2014-4-0835) to I.A., D.P., A.G., A.K.G., A.G.S., I.D.N., C.C.D., M.M., and D.C.D. K.K. was funded by the Japan Society for the Promotion of Science (KAKENHI Grant Numbers 18K06406, 19H02987).

Data availability Data used in the analyses presented here are available as Supplementary Information.

Code availability The Fractal Fragmentation and Disorder Index (FFDI) has been implemented as an open source ImageJ2/Fiji plugin in the ComsystanJ package, https://comsystan.github.io/comsystanj/ that can be downloaded from https://github.com/comsystan/comsystanj/tags.

Declarations

Conflict of interest The authors declare no conflict of interest or competing interests.

Ethical approval Not applicable.

Consent to participate Not applicable.

Consent for publication All authors have given consent to the publication of this manuscript.

References

Ahammer H (2011) Higuchi dimension of digital images. PLoS ONE 6:e24796

Andronache IC, Ahammer H, Jelinek HF et al (2016) Fractal analysis for studying the evolution of forests. Chaos Solitons Fract 91:310–318

Andronache I, Fensholt R, Ahammer H et al (2017) Assessment of textural differentiations in forest resources in Romania using fractal analysis. Forests 8:54

Andronache I, Marin M, Fischer R et al (2019) Dynamics of forest fragmentation and connectivity using particle and fractal analysis. Sci Rep 9:12228

Arroyo-Rodríguez V, Saldaña-Vázquez RA, Fahrig L, Santos BA (2017) Does forest fragmentation cause an increase in forest temperature? Ecol Res 32:81–88

Baker GL, Gollub JP (1996) Chaotic dynamics: an introduction, 2nd ed. Cambridge University Press, Cambridge

Balteanu D, Ielenicz M, Popescu N (1998) Geomorphology of the Romanian Carpathians. New trends and evolutions. Stud Geomorphol Carpatho-Balcan 32:89–109

Barnsley MF, Devaney RL, Mandelbrot BB et al (1988) The science of fractal images. Springer, New York

Batar AK, Shibata H, Watanabe T (2021) A novel approach for forest fragmentation susceptibility mapping and assessment: a case study from the Indian Himalayan Region. Remote Sens 13:4090

Benguigui L, Czamanski D, Marinov M, Portugali Y (2000) When and where is a city fractal? Environ Plann B Plann Des 27:507–519

Bianciardi G, Rizzo V, Cantasano N (2014) Opportunity Rover's image analysis: microbialites on Mars? Int J Aeronaut Space Sci 15:419–433

Bonan GB (2008) Forests and climate change: forcings, feedbacks, and the climate benefits of forests. Science 320:1444–1449

Borowska M, Borys K, Szarmach J, Oczeretko E (2017) Fractal dimension in textures analysis of xenotransplants. J VLSI Signal Process Syst Signal Image Video Technol 11:1461–1467

Boyce MS, Mallory CD, Morehouse AT et al (2017) Defining landscapes and scales to model landscape–organism interactions. Curr Landsc Ecol Rep 2:89–95

Cecílio RA, Pimentel SM, Zanetti SS (2019) Modeling the influence of forest cover on streamflows by different approaches. CATENA 178:49–58

Ciobotaru A-M, Andronache I, Ahammer H et al (2019) Recent deforestation pattern changes (2000–2017) in the central Carpathians: a gray-level co-occurrence matrix and fractal analysis approach. Forests 10:308

Coops NC, Hermosilla T, Wulder MA et al (2018) A thirty year, fine-scale, characterization of area burned in Canadian forests shows evidence of regionally increasing trends in the last decade. PLoS ONE 13:e0197218

Costanza JK, Riitters K, Vogt P, Wickham J (2019) Describing and analyzing landscape patterns: where are we now, and where are we going? Landsc Ecol 34:2049–2055

de Souza Lins Borba FK, Felix GLQ, Costa EVL et al (2016) Fractal analysis of extra-embryonic vessels of chick embryos under the effect of glucosamine and chondroitin sulfates. Microvasc Res 105:114–118

Diaconu DC, Andronache I, Pintilii R-D et al (2019) Using fractal fragmentation and compaction index in analysis of the deforestation process in Bucegi Mountains Group, Romania. Carpath J Earth Environ Sci 14:431–438

Drăghici CC, Andronache I, Ahammer H et al (2017) Spatial evolution of forest areas in the northern Carpathian Mountains of Romania. Acta Montanistica Slov 22:95–106

Eguiraun H, López-de-Ipiña K, Martinez I (2014) Application of entropy and fractal dimension analyses to the pattern recognition of contaminated fish responses in aquaculture. Entropy 16:6133–6151

Elith J, Leathwick JR (2009) Species distribution models: ecological explanation and prediction across space and time. Annu Rev Ecol Evol Syst 40:677–697

ESRI (2020) ArcGIS 10.8, Redlands. http://www.esri.com/software/arcgis/index.html. Accessed Oct 2020

Fabrizii M, Moinfar F, Jelinek HF et al (2014) Fractal analysis of cervical intraepithelial neoplasia. PLOS ONE 9:e108457

Fahrig L (2003) Effects of habitat fragmentation on biodiversity. Annu Rev Ecol Evol Syst. https://doi.org/10.1146/annurev.ecolsys.34.011802.132419

Fahrig L (2017) Ecological responses to habitat fragmentation per se. Annu Rev Ecol Evol Syst 48:1–23

Fischer R, Taubert F, Müller MS et al (2021) Accelerated forest fragmentation leads to critical increase in tropical forest edge area. Sci Adv 7:7012

Gao P, Cushman SA, Liu G et al (2019) FracL: a tool for characterizing the fractality of landscape gradients from a new perspective. ISPRS Int J Geo Inf 8:466

Gardner RH, O'Neill RV (1991) Pattern, process, and predictability: the use of neutral models for landscape analysis. In: Turner MG, Gardner RH (eds) Quantitative methods in landscape ecology: the analysis and interpretation of landscape heterogeneity. Springer, New York, pp 289–307

Gardner RH, Milne BT, Turnei MG, O'Neill RV (1987) Neutral models for the analysis of broad-scale landscape pattern. Landsc Ecol 1:19–28

Groffman PM, Baron JS, Blett T et al (2006) Ecological thresholds: the key to successful environmental management or an important concept with no practical application? Ecosystems 9:1–13

Gustafson EJ (2019) How has the state-of-the-art for quantification of landscape pattern advanced in the twenty-first century? Landsc Ecol 34:2065–2072

Haddad NM, Brudvig LA, Clobert J et al (2015) Habitat fragmentation and its lasting impact on Earth's ecosystems. Sci Adv 1:e1500052

Halley JM, Hartley S, Kallimanis AS et al (2004) Uses and abuses of fractal methodology in ecology. Ecol Lett 7:254–271

Hansen MC, Potapov PV, Moore R et al (2013) High-resolution global maps of 21st-century forest cover change. Science 342:850–853

Harte J, Newman EA (2014) Maximum information entropy: a foundation for ecological theory. Trends Ecol Evol 29:384–389

Homan RN, Windmiller BS, Reed JM (2004) Critical thresholds associated with habitat loss for two vernal pool-breeding amphibians. Ecol Appl 14:1547–1553
IBM Corp (2017) Released 2017. IBM SPSS statistics for windows, version 25.0. IBM Corp, Armonk
Jin XC, Ong SH, Jayasooriah (1995) A practical method for estimating fractal dimension. Pattern Recogn Lett 16:457–464
Joshi PK, Lele N, Agarwal SP (2006) Entropy as an indicator of fragmented landscape. Curr Sci 91:276–278
Kainz P, Mayrhofer-Reinhartshuber M, Ahammer H (2015) IQM: an extensible and portable open source application for image and signal analysis in Java. PLOS ONE 10(1):e0116329
Kareiva P (1987) Habitat fragmentation and the stability of predator–prey interactions. Nature 326:388–390
Kenkel N (2013) Sample size requirements for fractal dimension estimation. Community Ecol 14:144–152
Krummel JR, Gardner RH, Sugihara G et al (1987) Landscape patterns in a disturbed environment. Oikos 48:321–324
Kunicki ACB, Oliveira AJ, Mendonça MBM et al (2009) Can the fractal dimension be applied for the early diagnosis of non-proliferative diabetic retinopathy? Braz J Med Biol Res 42:930–934
Lavorel S, Chesson P (1995) How species with different regeneration niches coexist in patchy habitats with local disturbances. Oikos 74:103–114
Lavorel S, Gardner RH, O'Neill RV (1993) Analysis of patterns in hierarchically structured landscapes. Oikos 67:521–528
Liu J, Coomes DA, Gibson L et al (2019) Forest fragmentation in China and its effect on biodiversity. Biol Rev Camb Philos Soc 94:1636–1657
Loke LH, Chisholm RA (2022) Measuring habitat complexity and spatial heterogeneity in ecology. Ecol Lett 25:2269–2288
Ma D, Stoica AD, Wang X-L (2009) Power-law scaling and fractal nature of medium-range order in metallic glasses. Nat Mater 8:30–34
Macaluso D, Italia F, Bianciardi G (2015) Spreading of a colon adenoma: a case report. Fractal Geom Nonlinear Anal Med Biol 1:123–127
Mandal S, Mondal S (2019) Statistical approaches for landslide susceptibility assessment and prediction. Springer, Cham
Mandelbrot BB (1982) The fractal geometry of nature. Freeman Press, New York
Milne BT (1988) Measuring the fractal geometry of landscapes. Appl Math Comput 27:67–79
Milne BT (1992) Spatial aggregation and neutral models in fractal landscapes. Am Nat 139:32–57
Ministry of Water and Forests, Romanian Government (2017) Report on the state of Romania's forests in 2017. 10.6084/m9.figshare.20414397; http://www.mmediu.ro/app/webroot/uploads/files/Starea%20pădurilor2017.docx. Accessed 14 Oct 2019
Newman EA, Kennedy MC, Falk DA (2019) Scaling and complexity in landscape ecology. Front Ecol Evol 7:293
Newman EA, Wilber MQ, Kopper KE, Moritz MA (2020) Disturbance macroecology: a comparative study of community structure metrics in a high-severity disturbance regime. Ecosphere 11:e03022
Nowosad J, Stepinski TF (2019) Information theory as a consistent framework for quantification and classification of landscape patterns. Landsc Ecol 34:2091–2101
Park NW (2015) Using maximum entropy modeling for landslide susceptibility mapping with multiple geoenvironmental data sets. Environ Earth Sci 73:937–949
Phillips SJ, Dudík M, Schapire RE (2004) A maximum entropy approach to species distribution modeling. In: Proceedings of the twenty-first international conference on machine learning. Association for computing machinery, New York, p 83
Pintilii RD, Andronache I, Diaconu DC, Dobrea RC (2017) Using fractal analysis in modeling the dynamics of Forest areas and economic impact assessment: Maramureș County, Romania, as a case study. Forests 8:25
Plotnick RE, Gardner RH, O'Neill RV (1993) Lacunarity indices as measures of landscape texture. Landsc Ecol 8:201–211
Plotnick RE, Gardner RH, Hargrove WW et al (1996) Lacunarity analysis: a general technique for the analysis of spatial patterns. Phys Rev E Stat Phys Plasmas Fluids Relat Interdiscipl Top 53:5461–5468
Rényi A (1970) Probability theory. American Elsevier Publishing Company Inc, New York, p 366
Schneider CA, Rasband WS, Eliceiri KW (2012) NIH Image to ImageJ: 25 years of image analysis. Nat Methods 9:671–675
Shannon CE (1948) A mathematical theory of communication. Bell Syst Tech J 27:379–423
Shipley B, Vile D, Garnier E (2006) From plant traits to plant communities: a statistical mechanistic approach to biodiversity. Science 314:812–814
Song X-P, Hansen MC, Stehman SV et al (2018) Global land change from 1982 to 2016. Nature 560:639–643
Song Z, Seitz S, Li J et al (2019) Tree diversity reduced soil erosion by affecting tree canopy and biological soil crust development in a subtropical forest experiment. For Ecol Manage 444:69–77
Supp SR, Ernest SKM (2014) Species-level and community-level responses to disturbance: a cross-community analysis. Ecology 95:1717–1723
Tannier C, Pumain D (2005) Fractals in urban geography: a theoretical outline and an empirical example. Cybergeo. https://doi.org/10.4000/cybergeo.3275
Thompson I, Mackey B, McNulty S, Mosseler A (2009) Forest resilience, biodiversity, and climate change. In: Secretariat of the Convention on Biological Diversity, Montreal. Technical Series no. 43. fs.usda.gov, pp 1–67
Turner MG, Gardner RH (2015) Landscape metrics. Landscape ecology in theory and practice. Springer, New York, pp 97–142
Turner MG, Dale VH, Gardner RH (1989) Predicting across scales: theory development and testing. Landsc Ecol 3:245–252
Walters S (2007) Modeling scale-dependent landscape pattern, dispersal, and connectivity from the perspective of the organism. Landsc Ecol 22:867–881

Weber TC (2011) Maximum entropy modeling of mature hardwood forest distribution in four US states. For Ecol Manage 261:779–788
Wickham J, Riitters KH (2019) Influence of high-resolution data on the assessment of forest fragmentation. Landsc Ecol 34:2169–2182
Wiens JA, Stenseth NC, Van HorneIms BRA (1993) Ecological mechanisms and landscape ecology. Oikos 66:369–380
Wilson MC, Chen X-Y, Corlett RT et al (2016) Habitat fragmentation and biodiversity conservation: key findings and future challenges. Landsc Ecol 31:219–227
Wimberly MC (2006) Species dynamics in disturbed landscapes: when does a shifting habitat mosaic enhance connectivity? Landsc Ecol 21:35–46
With KA (1997) The application of neutral landscape models in conservation biology (Aplicacion de Modelos de Paisaje Neutros en la Biologia de la Conservacion). Conserv Biol 11:1069–1080
With KA (2002) The landscape ecology of invasive spread. Conserv Biol 16:1192–1203
With KA (2004) Assessing the risk of invasive spread in fragmented landscapes. Risk Anal 24:803–815
With KA, King AW (1997) The use and misuse of neutral landscape models in ecology. Oikos 79:219–229
With KA, King AW (1999) Extinction thresholds for species in fractal landscapes. Conserv Biol 13:314–326
With KA, King AW (2004) The effect of landscape structure on community self-organization and critical biodiversity. Ecol Modell 179:349–366
Wu J, David JL (2002) A spatially explicit hierarchical approach to modeling complex ecological systems: theory and applications. Ecol Modell 153:7–26
Yufeng S, Fengxiang J (2009) Landslide stability analysis based on generalized information entropy. In: 2009 International conference on environmental science and information application technology. ieeexplore.ieee.org, pp 83–85